Available online at www.sciencedirect.com
ScienceDirect
Trans. Nonferrous Met. Soc. China 35(2025) 640−652
Transactions of Nonferrous Metals Society of China
www.tnmsc.cn

Stepwise recovery of Zn, In, Ga, and Fe from jarosite residue through oxidizing roasting−direct reduction−smelting−electrorefining process

De-qing ZHU[1], Tao DONG[1], Jian PAN[1], Zhen-qi GUO[1], Cong-cong YANG[1], Yu-xiao XUE[2]

1. School of Minerals Processing and Bioengineering, Central South University, Changsha 410083, China;
2. College of Materials Science and Engineering, Chongqing University, Chongqing 400045, China

Received 11 May 2023; accepted 29 January 2024

Abstract: An efficient process based on oxidizing roasting−direct reduction−smelting−electrorefining was developed to separate and recover Zn, In, Ga and Fe from a typical hazardous jarosite residue. Phase transformation and element migration during each separating process were evaluated by X-ray diffraction analysis (XRD), thermo-gravimetric−differential scanning calorimetry (TG−DSC), and scanning electron microscopy−energy dispersive spectrometry (SEM−EDS). The results show that the jarosite residue decomposed into hematite and zinc ferrite when oxidizing roasted at 1250 °C for 20 min. Then, Zn and In were volatilized and enriched into flue dust through the reductive roasting of oxidized pellets at 1200 °C for 60 min. Finally, Fe and Ga were separated by smelting−electrorefining of the reduced pellets to obtain high purity iron powder with 99.5% Fe and anode slime with 456 g/t Ga. Through the process, a total recovery of 97.42% Zn, 87.86% In, 90.70% Fe and 84.78% Ga can be achieved.

Key words: jarosite residue; gallium; indium; recovery; electrorefining

1 Introduction

Due to diminishing reserves of primary metals and growing concerns about environmental degradation, considerable environmental attention has recently been focused on recovering valuable metals from solid wastes or secondary sources. Jarosite residue is a typical hazardous waste generated from hydrometallurgical routes to remove iron in the zinc extraction process [1,2]. A typical industrial plant usually generates 0.5−0.8 t of jarosite residue per ton production of metallic Zn. Despite its hazardous and toxic nature that requires safe disposal, it is also an important secondary resource that contains large quantities of valuables, including Fe, Ga, In, and Zn, etc. [3]. Recycling these valuable metals is significant for developing an environmentally friendly zinc processing route and ensuring a sustainable future.

Numerous processes have been developed for the recovery of valuable metals from the jarosite residue based on hydrometallurgy, pyrometallurgy, or a combination of both processes. Hydrometallurgical processes usually use different leaching agents to recover metal elements. The acid leaching process allows the dissolution of the acid-extractable metals and obtains a “clean” jarosite residue, which is operated immediately after precipitation or the beginning of recovery of metals in the zinc processing plant. Previous studies [4,5] reported that jarosite is a metastable phase at an extreme pH range (1.5<pH<2.5) and room temperature, according to E_h, pH, and activity diagrams. However, a few metals forming strong bonds with the residue may preclude extraction efficiency unless the phases of those metals can be transformed [6,7]. Some researchers applied other

Corresponding author: Cong-cong YANG, E-mail: smartyoung@csu.edu.cn
DOI: https://doi.org/10.1016/S1003-6326(24)66705-1

different leaching media to dissolve compounds, such as CN^- [8,9], HCl [10], H_2SO_4 [11,12], NaOH [13], $Ca(OH)_2$ [14,15], or bacterial [16]. However, current hydrometallurgical routes in industrial applications still require large reagent consumption for extraction of metals from the residue [17].

In contrast, pyrometallurgical processes are characterized by higher efficiency and larger scale to recover metals from jarosite residue. The jarosite residue can decompose at high temperatures and undergo phase transformation of complex jarosite into relatively simple metal oxides through dehydration, oxidization, and crystal transformation. This enables the liberation of valuable metals encapsulated or adsorbed by jarosite. Subsequently, flotation, magnetic separation and other techniques are employed to concentrate the iron and other valuable metals for efficient recovery of metal resources [18−20]. However, air pollution, high energy consumption, and extensive secondary waste restrict their practical application in the industry currently [21].

In our previous work [22], a pyrometallurgical route of oxidizing roasting−direct reduction−smelting was proposed for separation and recovery of Fe, Zn, In and Ga based on small-scale tests. In this work, the feasibility of the proposed pyrometallurgical route will be verified at pilot-scale. In addition, electrorefining was innovatively applied to separating Fe and Ga from Fe−Ga alloy. The mechanism of separation of Fe and Ga by the electrorefining process was studied through a series of analytical methods including Factsage8.0 thermodynamics calculation, X-ray diffraction (XRD), and scanning electron microscopy−energy dispersive spectrum analysis (SEM−EDS). This study aims to provide an essential reference for the comprehensive utilization of jarosite residue.

2 Experimental

2.1 Raw materials

The jarosite residue sample was provided by a zinc processing plant in southern China. It was dried for characterization in an oven at (105±5) °C to evaporate the free water. The main composition is listed in Table 1. It is known that the residue contains 12.6% S, 26.84% Fe, 3.74% Zn, 305 g/t In, and 82 g/t Ga. It is worth mentioning that its loss on ignition (LOI) is as high as 42.93%.

Figure 1 shows the main phases in the residue, including sodium jarosite ($NaFe_3(SO_4)_2(OH)_6$), $ZnSO_4·H_2O$, and $ZnSO_4·6H_2O$. The previous works [22] reported that preliminary roasting of the jarosite residue for decomposing and desulfurization is necessary and important to the subsequent separation and recovery of Fe, Zn, In and Ga.

Table 1 Chemical composition of jarosite residue (wt.%)

Zn	In[a]	Ga[a]	Ag[a]	Fe_T	SiO_2	CaO	MgO	Al_2O_3
3.74	305	82	73.5	26.84	0.89	0.29	0.44	1.67
S	K_2O	Na_2O	Cu	As	Pb	Cd	Cr	LOI
12.6	0.21	2.83	0.17	0.19	0.44	0.01	0.033	42.93

[a]: Unit in g/t; Fe_T: Total iron

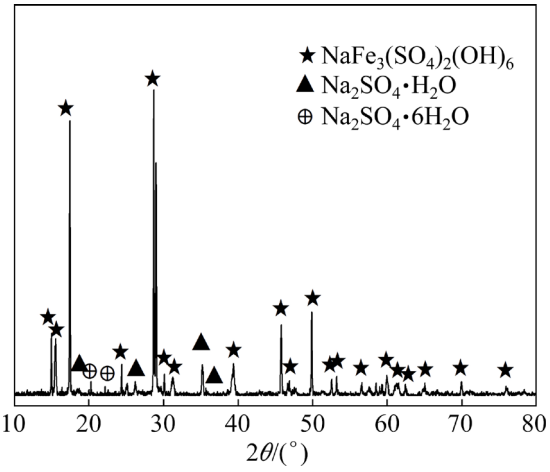

Fig. 1 XRD pattern of jarosite residue

Soft coal, with 52.12% fixed carbon, 30.41% volatile matter, and 4.49% ash, was crushed and sieved to below 5 mm and served as a reductant for direct reduction and smelting tests.

Pulverized limestone with 100% passing 0.075 mm was used to adjust the slag binary basicity (CaO/SiO_2) in the smelting tests. It contains 54.02% CaO, 0.85% SiO_2 and 0.76% MgO.

2.2 Experimental procedure

2.2.1 Pilot-scale oxidizing roasting of jarosite residue pellets

Jarosite residue and a certain proportion of bentonite were mixed, and pelletized into 15−20 mm green balls in a disc pelletizer with diameter of 1000 mm. Then, the green balls were loaded into a pot grate (*d*300 mm × 500 mm, Fig. S1(a) in Supporting

Information (SI)) to simulate the straight grate pelletizing process to prepare fired pellets with sufficiently low S content. The temperature profile and air flow rate used in the oxidizing roasting tests are shown in Fig. 2. The jarosite residue pellets were roasted at 1250 °C for 20 min to quickly remove sulfate and consolidate pellets to achieve desirable mechanical strength [22,23]. The gaseous SO_x from decomposition of sulfates can be recovered to produce sulfuric acid.

The removal rate (R) of S during oxidizing roasting was calculated by

$$R=[(m_0^{\mathrm{r}}S_0-m_1^{\mathrm{r}}S_1)/(m_0^{\mathrm{r}}S_0)]\times100\% \quad (1)$$

where m_0^{r} and m_1^{r} are the dry mass of pellets before and after roasting, and S_0 and S_1 represent the S content of the pellets before and after roasting, respectively.

Usually, the less the S content in the fired pellets is, the higher the volatizing rate of Zn and In can be achieved in the subsequent direct direction process of the fired pellets.

2.2.2 Pilot-scale direct reduction of fired pellets

The fired pellets were directly reduced in a pilot-scale rotary kiln (d1000 mm × 500 mm, Fig. S1(b) in SI) to volatilize Zn and In into the flue gas, while Fe and Ga were retained in the reduced pellets [24]. Approximately 15 kg fired pellets and a measured quantity of soft coal were charged into the kiln quickly, and the remnant soft coal was divided into three parts and loaded in 15, 30, and 45 min, respectively, by a screw feeder. The reduction temperature was controlled by adjusting the flow rate of natural gas and air. After direct reduction, the hot-reduced pellets were immediately removed from the kiln, and loaded into a sealed tank with gas nitrogen injection to prevent further oxidation. The tank was put in the cold water to cool down to room temperature.

The mass of the pellets before and after reduction was weighed and recorded. The content of total Fe, Zn, In and Ga was assayed to calculate the metallization degree and volatilization rates. The metallization degree of iron (γ) was determined using

$$\gamma=M_{\mathrm{Fe}}/M_{\mathrm{Fe}}^{\mathrm{T}}\times100\% \quad (2)$$

where M_{Fe} and $M_{\mathrm{Fe}}^{\mathrm{T}}$ are the contents of metallic Fe and the total Fe of the reduced pellets, respectively.

The volatilization rates of Zn and In (v_{Me}) were determined using

$$v_{\mathrm{Me}}=[(m_{\mathrm{r1}}\alpha_{\mathrm{r1}}-m_{\mathrm{r2}}\alpha_{\mathrm{r2}})/(m_{\mathrm{r1}}\alpha_{\mathrm{r1}})]\times100\% \quad (3)$$

where m_{r1} and m_{r2} represent the mass of the pellets before and after reduction, respectively; α_{r1} and α_{r2} are the original and residual content of Zn (or In, Ga) metal elements in the pellets before and after reduction, respectively.

2.2.3 Smelting of reduced pellets to manufacture Fe−Ga alloy

The smelting tests were conducted in a muffle furnace under N_2 atmosphere with $MoSi_2$ heating (Fig. S2 in SI). Approximately 200 g reduced pellets were mixed with limestone and then loaded into a graphite crucible (d75 mm × 100 mm). Its mass was determined according to a fixed basicity (CaO/SiO_2) of 0.8. In smelting tests, the crucible was moved into the heat zone of the furnace and then held for 20 min. At the end of the smelting process, the crucible was taken out and then covered

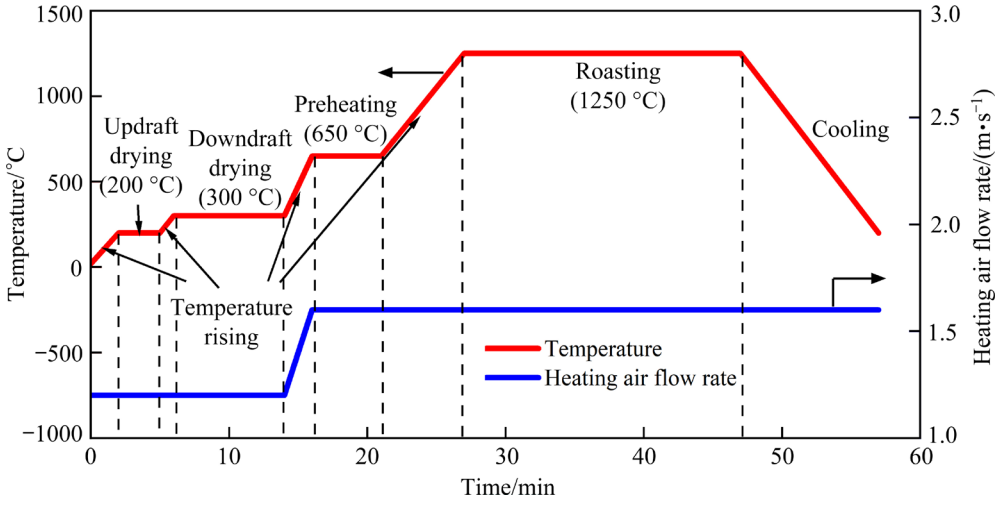

Fig. 2 Temperature profile and heating air flow rate of pilot-scale roasting tests of jarosite residue pellets

by coal to cool to room temperature. The alloy and slag were separated manually and weighed.

The recovery rates (η_{Me}) of Fe and Ga were determined using

$$\eta_{Me}=[m_{s2}\alpha_{s2}/(m_{s1}\alpha_{s1})]\times100\% \quad (4)$$

where m_{s1} and m_{s2} represent the mass of reduced pellets before smelting and alloy obtained, respectively; α_{s1} is the original Fe (or Ga) content in the reduced pellets while α_{s2} is the Fe (or Ga) content in the alloy.

The above smelting tests were repeated under optimal smelting conditions to prepare enough alloy samples for subsequent electrorefining tests. About 10 kg Fe−Ga alloy was manufactured and put into an induction furnace (Fig. S3 in SI) with a graphitic crucible (120 mm × 120 mm × 140 mm) for remelting at (1500±5) °C for 180 min under N_2 atmosphere. Finally, a cuboidal Fe−Ga alloy ingot (Fig. S4 in SI) with uniform chemical composition was obtained.

To confirm the safety of the final slag rejected from the smelting process, the toxicity characteristic leaching procedure (TCLP) tests were carried out by following the standard leaching procedure released by the Environmental Protection Agency (EPA).

2.2.4 Electrorefining of Fe−Ga alloy to separate Fe and Ga

The cuboidal alloy ingot was cut into square slices (Fig. S5(a) in SI, 100 mm × 100 mm × 3 mm), and then polished as an anode plate. The cathode plate (Fig. S5(b) in SI, 110 mm × 110 mm × 2 mm) was made of austenitic 304 stainless steel plates. Both cathode and anode plates were immersed in the electrolyte of $FeSO_4$−$(NH_4)_2SO_4$. The pH of electrolyte was maintained at around 4 by adjusting sulfuric acid addition for the entire 12 h electrorefining procedure for each cathode plate.

A microcomputer-control DC power rectifier was used to control DC electricity at output voltage of 0−15 V and current of 0−30 A within the electrorefining cell. Iron powder was collected from the cathode plate and immediately rinsed with deionized water 20 times. The obtained iron powder and anode slime were separately dried, weighed, and analyzed at the end of the procedure.

The evaluation indexes of the electrorefining process for the separation of Fe and Ga in the alloy are shown in Eqs. (5)−(7):

$$P=M/(St) \quad (5)$$

$$E=M/(1042It)\times100\% \quad (6)$$

$$f=V/(1.042E)\times1000 \quad (7)$$

where P represents the productivity of Fe powder, g/(m^2·h); E represents the current efficiency, %; f represents electricity consumption, kW·h/t; M represents the iron powder mass in a period, g; I represents average current in a period, A; V represents voltage in a period, V; t represents the electrorefining duration, h; S represents the area of the cathode plate, m^2.

2.2.5 Characterization of materials in process

The chemical compositions of the samples from different stages were measured by chemical titration method. The phase analysis of the materials was performed by an X-ray diffractometer (XRD, SIEMENS D500, Brugg Group, Switzerland). The microstructure of the samples in different processes was demonstrated by a scanning electron microscope (SEM, FEI Quanta 200, FEI, Finland) and energy dispersive spectrometer (EDS, EDAX32, Mahwah, NJ, USA). The thermogravimetric analysis and differential scanning calorimetry (TG−DSC, STA-449C, NETZSCH, Germany) experiment of jarosite residue was carried out in N_2 atmosphere with a flow rate of 50 mL/min. The temperature was 30−1000 °C, and the heating rate was 5 °C/min.

3 Results and discussion

3.1 Oxidizing roasting of jarosite residue pellets

According to the previous studies [22], Zn and In occur primarily in sulfide and sulfate and are difficult to be reduced by carbon. Consequently, the volatilization rate of Zn and In in jarosite residue is low in the case of direct reduction without preliminary removal of S. Therefore, it is critical to eliminate sulfur by oxidizing roasting.

As shown in Fig. 3 and Fig. S6 in SI, the mass loss of jarosite can be divided into three stages. The first mass loss is observed for jarosite at 30−426 °C. There is a strong endothermic peak at about 413 °C, which is caused by the decomposition of jarosite. The reaction equation in this stage can be described as follows:

$$2NaFe_3(SO_4)_2(OH)_6= Na_2SO_4+Fe_2(SO_4)_3+Fe_2O_3+6H_2O\uparrow \quad (8)$$

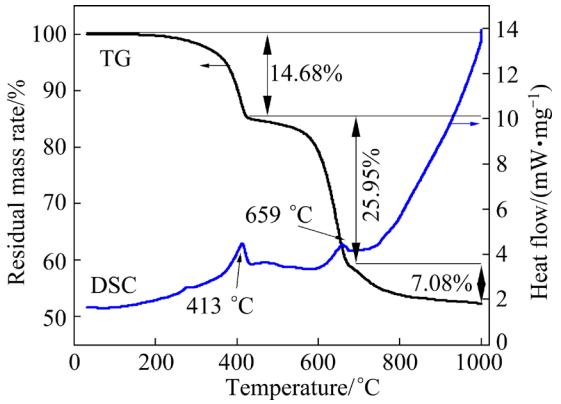

Fig. 3 TG−DSC curve of jarosite residue

The second mass loss stage begins at 426 °C and ends at 680 °C. There is an endothermic peak at about 659 °C, which is caused by the decomposition of ferric sulfate:

$$Fe_2(SO_4)_3=Fe_2O_3+3SO_2\uparrow+3/2O_2\uparrow \quad (9)$$

$$2FeSO_4=Fe_2O_3+2SO_2\uparrow+1/2O_2\uparrow \quad (10)$$

The third mass loss takes place from 680 to 1000 °C, which is attributed to the decomposition of $ZnSO_4$ and Na_2SO_4. The decomposition of $ZnSO_4$ is at 985 °C (Eqs. (11) and (12)), which exhibits higher thermal stability and requires higher decomposition temperature [25,26]. The reactions in this stage can be described as follows:

$$ZnSO_4=ZnO+SO_2\uparrow+1/2O_2\uparrow \quad (11)$$

$$ZnSO_4+Fe_2O_3=ZnFe_2O_4+SO_2\uparrow+1/2O_2\uparrow \quad (12)$$

$$Na_2SO_4=2Na\uparrow+SO_2\uparrow+O_2\uparrow \quad (13)$$

$$Na_2SO_4(s/l)\ =Na_2SO_4\uparrow \quad (14)$$

Table 2 gives the chemical composition of the fired pellets obtained under conditions of roasting at 1250 °C for 20 min. The contents of Fe, Zn, In and Ga increase from 26.84%, 3.74%, 305 g/t and 82 g/t to 49.28%, 6.87%, 560 g/t and 150 g/t, respectively. It is noteworthy that the residual S content drops from 12.6% to 0.9%, and the desulfurization rate reaches approximately 96%, similar to that in the small-scale firing tests (98.53%).

Figure 4 presents the XRD pattern of the fired pellets. The main phases can be identified, i.e., Zn ferrite ($ZnFe_2O_4$) and hematite (Fe_2O_3), indicating that jarosite has decomposed completely under the given roasting conditions. Moreover, a small quantity of Na_2SO_4 phase is still detected, suggesting that residual S is probably in the form of Na_2SO_4.

Table 2 Chemical composition of fired pellets from pilot-scale pot grate (wt.%)

Zn	In[a]	Ga[a]	Fe_T	K_2O	Na_2O	Pb
6.87	560	150	49.28	0.39	0.24	0.35
As	SiO_2	CaO	MgO	Al_2O_3	S	
0.23	5.9	0.42	0.73	3.52	0.9	

[a]: Unit in g/t

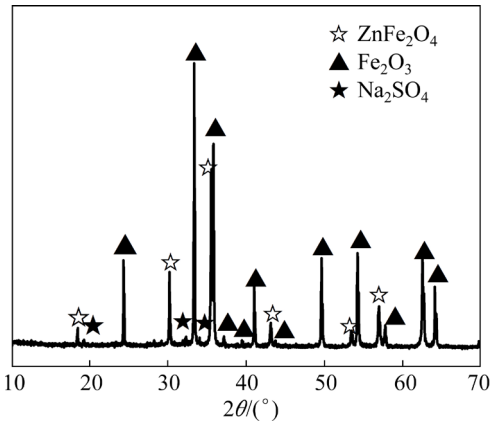

Fig. 4 XRD pattern of fired pellets from pilot-scale tests

3.2 Direct reduction of fired pellets

According to small-scale tests [22], increasing the reduction temperature and prolonging the reduction time improve the volatilization of Zn and In. The volatilizations are nearly 100% and approximately 85% when reduced at 1200 °C for 70 min and with a total C/Fe mole ratio of 1.82. In the current work, the volatilization rates of Zn and In reached 97.4% and 87.8%, respectively. The results indicate that Zn and In can be effectively separated from reduced pellets by applying direct reduction technique.

Figures 5 and 6 show the XRD pattern and SEM−EDS analysis of the Zn-bearing dust in the direct reduction process. The main occurrence of Zn in the dust is free ZnO, and other phases are not detected due to their low content. Combined with the SEM−EDS analysis, the ZnO particles have a small size of 100 nm in a regular hexahedral structure or dendritic shape. The dust can be further subjected to pyro- and hydro-metallurgical processes for purification and metal recovery.

The chemical composition of the reduced pellets from the pilot-scale tests is listed in Table 3. It is known that the reduced pellets contain 83.34% Fe, 255 g/t Ga, and a small amount of gangue (SiO_2, Al_2O_3, CaO, MgO, etc.), and the iron metallization ratio reaches 94.32%.

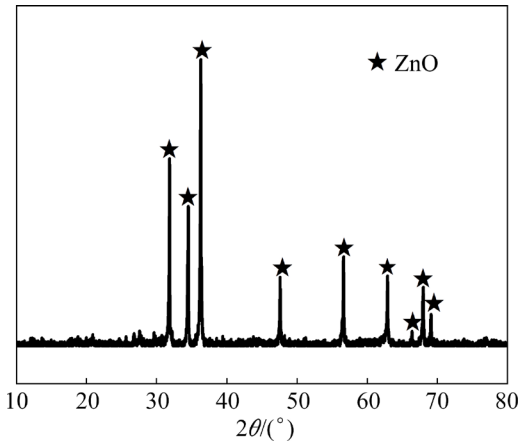

Fig. 5 XRD pattern of Zn-bearing dust processed via pilot-scale direct reduction

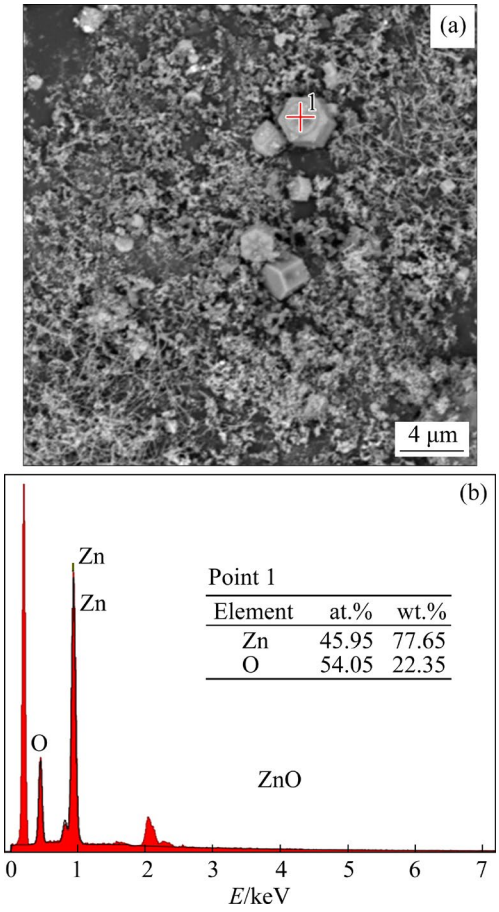

Fig. 6 SEM image (a) and Zn-bearing dust with EDS analysis of major phases (b)

Table 3 Chemical composition of reduced pellets processed via direct reduction (wt.%)

Fe_T	Fe_m	Zn	In[a]	Ga[a]	SiO_2	CaO	MgO	Al_2O_3
83.34	78.61	0.30	115	255	7.57	0.72	1.24	4.25

[a]: Unit in g/t; Fe_m: Metallic iron

3.3 Smelting of reduced pellets

Owing to good chemical affinity between Fe and Ga, Ga is enriched primarily in the liquid Fe and recovered in the form of Fe−Ga alloy during smelting of the reduced pellets [27]. The reduced pellets were smelted at 1550 °C for 20 min with a basicity of 0.8, and the recovery rates of Fe and Ga are 91.51% and 90.78%, respectively. The chemical compositions of alloy and slag are shown in Table 4. The Fe−Ga alloy contains 94.70% Fe and 287 g/t Ga. The molten alloy can be further refined to produce stainless steel or other steel directly.

Ga has been widely applied to manufacturing advanced semiconductors, mobile phones, optical communication devices, and computers because of its unique properties [28]. But Ga usually presents low content (average concentration is about 50×10^{-6}) in bauxite, Zn ores, and coals [29]. Here, Ga will be further enriched by electrorefining. Moreover, these lump alloys are remelted and cast into standard shapes to ensure uniform chemical composition.

After remelting of the Fe−Ga alloy, the Fe and Ga contents decrease from 94.70% and 287 g/t to 91.15% and 275 g/t, respectively, because the carbon of the reactor graphite crucible carbonizes into the alloy at high temperature for a long time. Fortunately, this phenomenon can be eliminated during direct casting under real industrial conditions.

The slag from the smelting of reduced pellets contains 36.35% Fe, 12.49% SiO_2 and 16.04% Al_2O_3, as shown in Table 4. To check the stability and toxicity of the slag, leaching tests were conducted according to the standard 1311 of TCLP. The results of the TCLP are list in Table 5. The TCLP test

Table 4 Chemical composition of Fe−Ga alloy and slag from smelting tests (wt.%)

Sample	Fe_T	Zn	In[a]	Ga[a]	C	SiO_2	CaO	MgO	Al_2O_3
Alloy	94.70	0.08	90.2	287	1.21	0.14	0.13	0.15	0.12
Cuboidal ingot	91.15	0.01	78.1	275	6.76	0.13	0.12	0.14	0.12
Slag	36.35	1.01	96.3	75.6	–	12.49	9.98	9.43	16.04

[a]: Unit in g/t

shows that the concentrations of heavy metals in the extraction solution are lower than the regular limits of the US-EPA, indicating that the slag is very stable and can be considered as non-hazardous waste, which can be stored or used for cement industry.

Table 5 Comparison of ion concentration in leaching solution of smelting slag with limit concentration of TCLP standard concentration (mg/L)

Item	As	Cd	Cr	Pb	Zn
Leachate	0.066	0.001	0.033	0.002	0.010
US-EPA	0.5	0.05	0.33	0.15	70

3.4 Electrorefining of Fe−Ga alloy

3.4.1 Parameter optimization of electrorefining process

Understanding the solution chemistry is a crucial step in optimizing electrorefining performance. Figure 7(a) shows a φ−pH diagram of the Fe−Ga−H_2O system at 25 °C, and it was built by Factsage ver. 8.0. Based on the results, Fe is in the form of Fe^{2+} ions dissolved in the solution while Ga is in the form of $Ga(OH)_3$(s) precipitating into the anode slime, indicating that Fe and Ga can be separated effectively by controlling the pH and φ in Fig. 7(a).

From Fig. 7(b), iron powder productivity, current efficiency, and electricity consumption increase significantly when the current density is increased from 100 to 200 A/m^2. The current density is a crucial parameter for electrorefining because a relatively high current density promotes the migration of Fe^{2+} ions in the electrolyte. However, further increasing the current density had a strong negative impact on the above index. The dendrites on the cathode edges appear, resulting in a short circuit in the cathode, and excess current is wasted. Therefore, a suitable current density is recommended at 200 A/m^2.

The effect of electrode spacing on iron powder productivity, current efficiency and electricity consumption is shown in Fig. 7(c) under the conditions of a current density of 200 A/m^2, Fe^{2+} concentration of 50 g/L and pH of 4.0. The iron powder productivity and current efficiency are increased from 265.29 to 279.34 g/(m^2·h), 92.19% to 97.07%, respectively, by elevating the electrode spacing from 40 to 60 mm. Further increase in the electrode spacing results in a decrease in iron

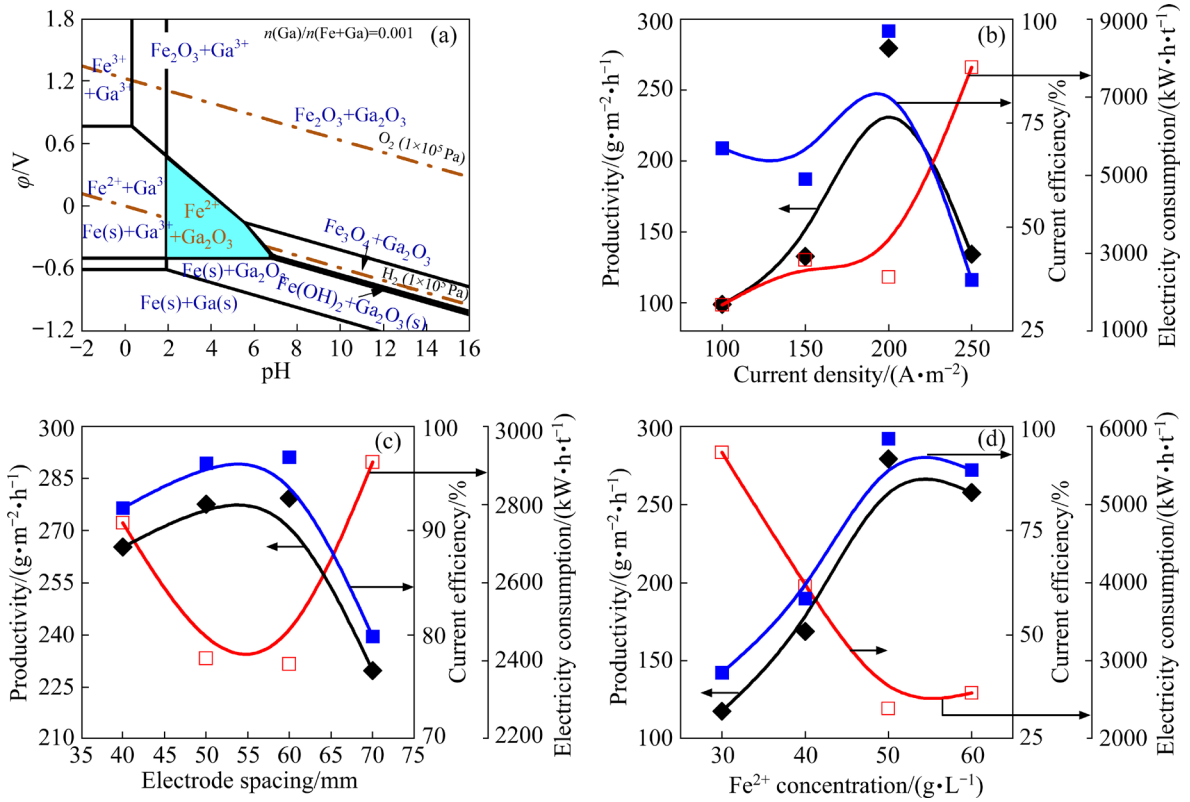

Fig. 7 φ−pH diagram for Fe−Ga−H_2O system at 25 °C (a), effect of current density (b), electrode spacing (c) and Fe^{2+} concentration (d) on electrorefining process

powder productivity and a noticeable increase in electricity consumption. A short circuit between the anode and the cathode may happen if the electrode spacing is too small. When electrode spacing widens significantly, the specific energy consumption will grow as well [30]. In this work, the optimum electrode spacing is suggested at 60 mm.

The effect of Fe^{2+} concentration on the current efficiency, electricity consumption and iron powder productivity was studied under the conditions of a current density of 200 A/m^2, an electrode spacing of 60 mm and pH of 4.0. (Fig. 7(d)). Increasing Fe^{2+} concentration has a strong positive effect on the iron powder productivity, current efficiency and electricity consumption, as higher Fe^{2+} concentration reduces electrolyte resistance and enhances ions migration. When the Fe^{2+} concentration increases from 30 to 50 g/L, the iron powder productivity and current efficiency improve from 117.93 to 279.34 g/(m^2·h) and 40.98% to 97.07%, respectively. Meanwhile, electricity consumption decreases from 5667 to 2392 kW·h/t. However, excessive Fe^{2+} concentration of electrolyte may induce unexpected morphologies of iron dendrites and potential risk of short circuit in the electrorefining process. Therefore, the appropriate Fe^{2+} concentration is suggested to be 50−60 g/L.

Therefore, the effective separation of Fe and Ga was achieved by electrorefining Fe−Ga alloy at an current efficiency of 97.07% and electricity consumption of 2392 kW·h/t. The iron powder productivity of electrorefining can be obtained at 279.34 g/(m^2·h) under the conditions of a current density of 200 A/m^2, electrode spacing of 60 mm in the electrolyte of 50 g/L Fe^{2+} and pH of 4.0.

The chemical compositions of the product obtained in this study are shown in Table 6. Pure iron powder can be used as feed for powder metallurgy. The main contents of the anode slime are 62.21% C and 9.20% Fe. Ga is enriched from 287 g/t in alloy to 456 g/t in anode slime. It is worth noting that In content is also enriched from 78.1 g/t in alloy to 187 g/t in anode slime. Ga enrichment goal is achieved. However, Ga grade is diluted significantly due to carbonization (Fig. 8) during ingot preparation, which can be improved in the future. If the carbon can be removed, the Ga content can be enriched up to 1207 g/t theoretically.

3.4.2 Electrolysis mechanism

The transfer includes mass and electron transfers during the electrolysis of Fe−Ga alloy, which is explained in Fig. 9.

In the anode, Fe preferentially lost electrons to become Fe^{2+} (Eq. (15)) and reacted with SO_4^{2-} to form $FeSO_4$ leaching into the electrolyte. Ga and other metals are also dissolved into electrolyte near anode in the form of Ga^{3+} and other ions (Eqs. (16) and (17)). H^+ ions are produced by H_2O reaction (Eq. (18)).

$$Fe-2e=Fe^{2+} \quad (15)$$

$$Ga-3e=Ga^{3+} \quad (16)$$

$$Zn-2e=Zn^{2+} \quad (17)$$

$$2H_2O-4e=4H^++O_2\uparrow \quad (18)$$

Here, the main components of the electrolyte are Fe^{2+}, NH_4^+, SO_4^{2-}, H^+, Ga^{3+} and H_2O. The Fe^{2+}, H^+, NH_4^+ and Ga^{3+} ions are driven by direct current and move toward the cathode. But some Fe^{2+} and most Ga^{3+} ions react with OH^- to form precipitate $Fe(OH)_2$ (Eq. (19)) and GaOOH (Eq. (20)) or $Ga(OH)_3$ (Eq. (21)), which further settle with some impurities (e.g., C and SiO_2) of anode as anode slime. Unstable $Fe(OH)_2$ is further oxidized by O_2 in the electrolyte to form $[Fe(II)_4Fe(III)_2(OH)_{12}]^{2+}$ [31,32] (Eq. (22)), Fe_3O_4 (Eq. (23)), FeOOH (Eq. (24)), and Fe_2O_3 (Eq. (25)), while SO_4^{2-} and OH^- ions move toward the anode.

$$Fe^{2+}+2OH^-=Fe(OH)_2\downarrow \quad (19)$$

$$Ga^{3+}+3OH^-=Ga(OH)_3\downarrow \quad (20)$$

$$Ga^{3+}+3OH^-=GaOOH\downarrow+H_2O \quad (21)$$

Table 6 Chemical composition of electrolytic iron powder and anode slime (wt.%)

Sample	Fe_T	Zn	In[a]	Ga[a]	SiO_2	Al_2O_3	CaO	MgO	C	S
Anode slime	9.20	0.02	187	456	1.21	1.33	1.45	1.78	62.21	3.21
Electrolytic iron powder	99.50	0.038	2.29	18.7	–	–	–	–	–	–

[a]: Unit in g/t

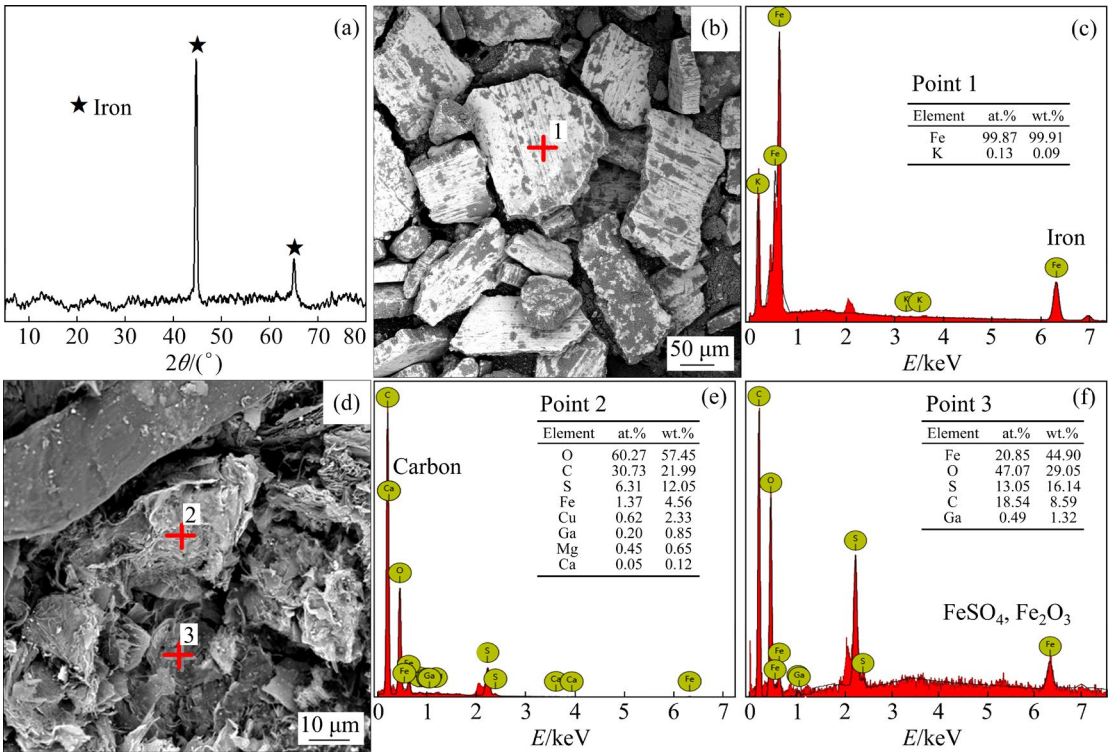

Fig. 8 XRD pattern (a) and SEM image (b) of electrolytic iron powder with EDS analysis (c), and SEM image (d) and EDS analysis (e, f) of anode slime

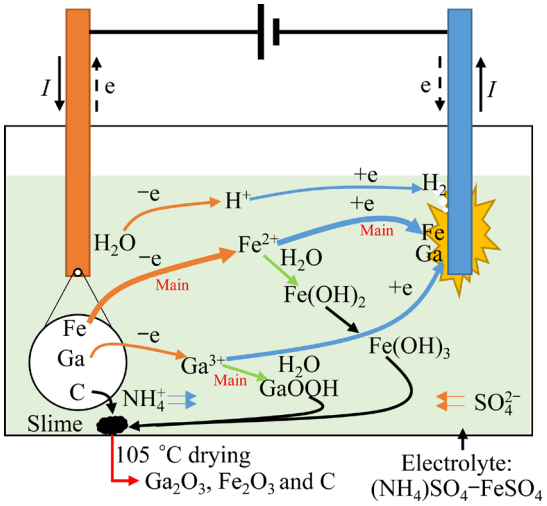

Fig. 9 Mechanism of designed electrolysis process

$$6Fe(OH)_2+O_2+4H^+=2H_2O+[Fe(II)_4Fe(III)_2(OH)_{12}]^{2+} \quad (22)$$

$$[Fe(II)_4Fe(III)_2(OH)_{12}]^{2+}=4H_2O+4H^++2Fe_3O_4 \quad (23)$$

$$4Fe_3O_4+6H_2O+O_2=12FeOOH \quad (24)$$

$$2FeOOH=Fe_2O_3+H_2O \quad (25)$$

Fe^{2+} ions gain electrons to form Fe (Eq. (26)) near the cathode, while a few H^+ ions also gain electrons to form H_2 (Eq. (27)), causing the pH of electrolyte to gradually increase.

$$Fe^{2+}+2e=Fe \quad (26)$$

$$2H^++2e=H_2\uparrow \quad (27)$$

3.5 Element mass balance of main metals in full flow sheet

Based on the tests mentioned above, a stepwise extraction full flowsheet for recovering Zn, In, Fe and Ga from jarosite is shown in Fig. 10. Zn and In are recovered as dust collected from flue gas, and the recovery rates are 97.42% and 87.86%, respectively. Fe is recovered as powder assaying 99.50% Fe, with a recovery rate of 90.70%. However, Ga is recovered as anode slime containing 456 g/t Ga with a recovery rate of 12.99%. Because 74.80% Ga (calculated) ions must saturate the liquor firstly according to Fig.S7 in SI, which are drawn by the Medusa software when the alloy is whole dissolving and the concentration of Ga ion reaches 2.36×10^{-4} mol/L. Considering electrorefining is continuous in practice, the initial electrolyte is composed of saturated Ga ions, and 71.79% Ga (actual) in the solution will be recovered as precipitate of $Ga(OH)_3$. Then, the total recovery rate of Ga can reach up to 84.78% (71.79%+12.99%).

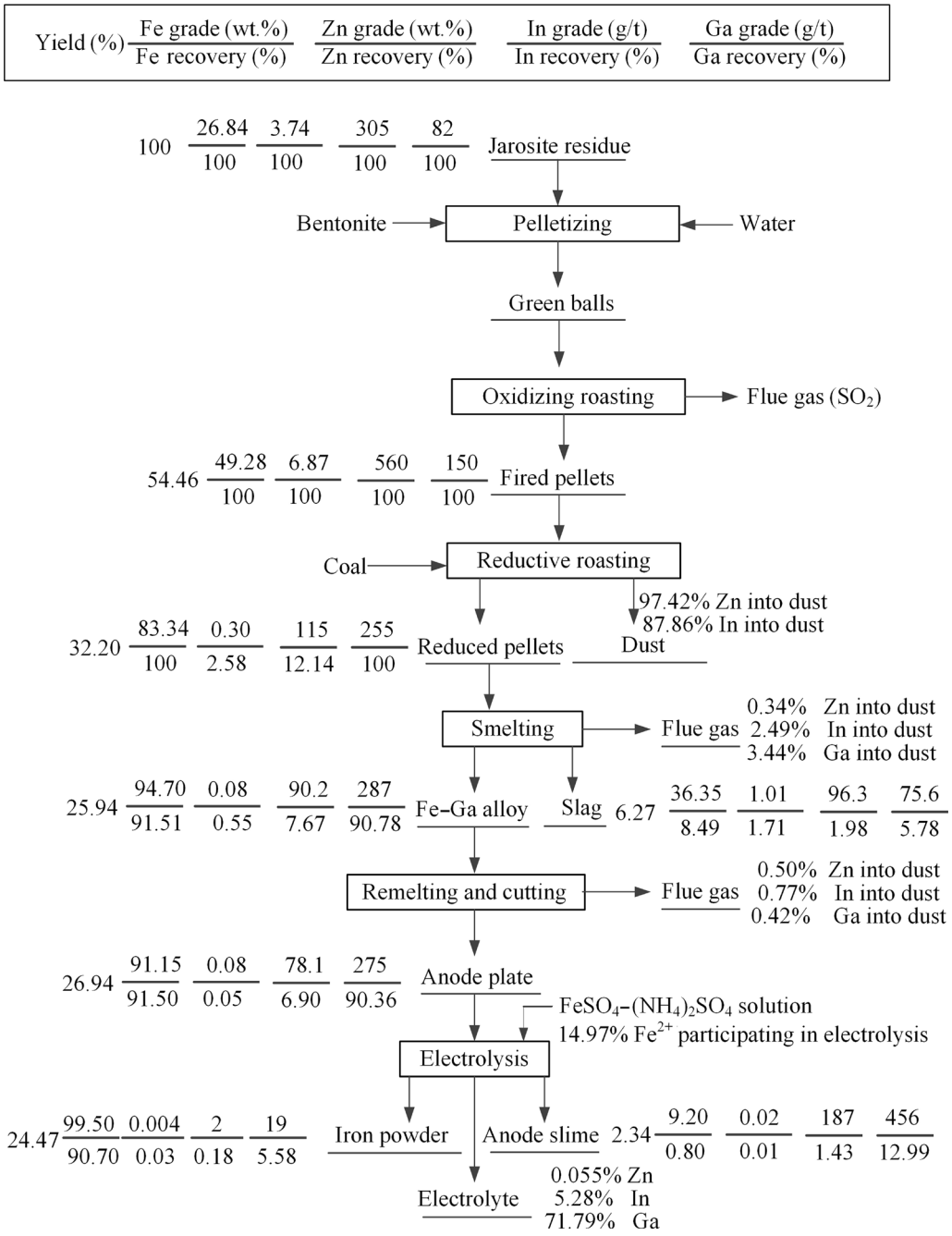

Fig. 10 Mass balance of main metals in full flowsheet of processing jarosite residue

The proposed innovative flowsheet for extracting valuable metals from jarosite residue is highly efficient. The main valuable metals, such as Fe, Zn, In and Ga are extracted and recovered from jarosite residue. No secondary hazardous wastes are rejected, indicating that it is a clean and green process.

4 Conclusions

(1) Green pellets made of jarosite residue should be oxidizing roasted to remove sulfur for effective volatilization of Zn and In by avoiding formation of nonvolatile sulfides. In the direct reduction process of the oxidized pellets, 0.9% S, 97.4% Zn and 87.8% In are recovered from the flue gas when reduced at 1200 °C for 60 min with a total C/Fe mole ratio of 1.82.

(2) In the smelting process of the reduced pellets, 91.50% Fe and 90.78% Ga are enriched to form Fe−Ga alloy under the conditions of smelting at 1550 °C for 20 min and slag basicity of 0.8. The slag has been proven to be safe by leaching toxicity tests and can be used as raw materials for cement or

storage.

(3) High-purity iron powder, assaying 99.50% Fe, can be obtained from electrorefining of the Fe−Ga alloy under the current density of 200 A/m^2, electrolyte concentration of 50 g/L Fe^{2+} and pH of 4.0. Meanwhile, Ga is mainly enriched in anode slime with a total recovery rate of 84.78% for further hydrometallurgical extraction.

(4) The developed process provides a potential way to extract and separate Zn, In, Fe and Ga from jarosite residue without rejection of hazardous waste. Further verification at industrial scale is necessary and meaningful in the future.

CRediT authorship contribution statement

De-qing ZHU: Conceptualization, Writing − Review & editing; **Tao DONG:** Writing − Original draft, Methodology; **Jian PAN** and **Zheng-qi GUO:** Project administration, Visualization; **Cong-cong YANG:** Funding acquisition, Resources, Validation supervision; **Yu-xiao XUE:** Investigation, Software.

Declaration of competing interest

The authors declare that they have no known competing financial interests or personal relationships that could have appeared to influence the work reported in this paper.

Acknowledgments

We would like express our sincere gratitude to the financial support from Hunan Provincial Key Research and Development Project, China (No. 2022SK2075), and the National Natural Science Foundation of China (No. 52004339).

Supplementary Information

Supplementary Information in this paper can be found at: http://tnmsc.csu.edu.cn/download/22-p0640-2023-0527-Supplementary_Information.pdf.

References

[1] AGUILAR-CARRILLO J, VILLALOBOS M, PI-PUIG T, ESCOBAR-QUIROZ I N, ROMERO F M. Synergistic arsenic (v) and lead (ii) retention on synthetic jarosite. I. Simultaneous structural incorporation behaviour and mechanism [J]. Environmental Science: Processes & Impacts, 2018, 20(2): 354−369.

[2] KEROLLI-MUSTAFA M, FAJKOVIC H, RONCEVIC S, CURKOVIC L. Assessment of metal risks from different depths of jarosite tailing waste of Trepca Zinc Industry, Kosovo based on BCR procedure [J]. Journal of Geochemical Exploration, 2015, 148: 161−168.

[3] HAN Hai-sheng, SUN Wei, HU Yue-hua, JIA Bao-liang, TANG Hong-hu. Anglesite and silver recovery from jarosite residues through roasting and sulfidization-flotation in zinc hydrometallurgy [J]. Journal of Hazardous Materials, 2014, 278: 49−54.

[4] CALLA-CHOQUE D, LAPIDUS G-T. Acid decomposition and silver leaching with thiourea and oxalate from an industrial jarosite sample [J]. Hydrometallurgy, 2020, 192: 105289.

[5] PALDEN T, REGADÍO M, ONGHENA B, BINNEMANS K. Selective metal recovery from jarosite residue by leaching with acid-equilibrated ionic liquids and precipitation-stripping [J]. ACS Sustainable Chemistry & Engineering, 2019, 7(4): 4239−4246.

[6] FORRAY F L, SMITH A M L, DROUET C, NAVROTSKY A, WRIGHT K, HUDSON-EDWARDS K A, DUBBIN W E. Synthesis, characterization and thermochemistry of a Pb-jarosite [J]. Geochimica et Cosmochimica Acta, 2010, 74(1): 215−224.

[7] HUDSON-EDWARDS K A, SMITH A M L, DUBBIN W E, BENNETT A J, MURPHY P J, WRIGHT K. Comparison of the structures of natural and synthetic Pb−Cu-jarosite-type compounds [J]. European Journal of Mineralogy, 2008, 20(2): 241−252.

[8] GONZÁLEZ-IBARRA A A, NAVA-ALONSO F, URIBE-SALAS A, CASTILLO-VENTUREÑO E N. Decomposition kinetics of industrial jarosite in alkaline media for the recovery of precious metals by cyanidation [J]. Canadian Metallurgical Quarterly, 2016, 55(4): 448−454.

[9] PELINO M. Recycling of zinc-hydrometallurgy wastes in glass and glass ceramic materials [J]. Waste Management, 2000, 20(7): 561−568.

[10] WANG Fen, YU Jun-xia, XIONG Wan-li, XU Yuan-lai, CHI Ru-an. A two-step leaching method designed based on chemical fraction distribution of the heavy metals for selective leaching of Cd, Zn, Cu, and Pb from metallurgical sludge [J]. Environmental Science and Pollution Research, 2018, 25(2): 1752−1765.

[11] REYES I A, MIRELES I, PATIÑO F, PANDIYAN T, FLORES M U, PALACIOS E G, GUTIÉRREZ E J, REYES M. A study on the dissolution rates of K−Cr(VI)-jarosites: kinetic analysis and implications [J]. Geochemical Transactions, 2016, 17: 3.

[12] REYES I A, PATIÑO F, FLORES M U, PANDIYAN T, CRUZ R, GUTIÉRREZ E J, REYES M, FLORES V H. Dissolution rates of jarosite-type compounds in H_2SO_4 medium: A kinetic analysis and its importance on the recovery of metal values from hydrometallurgical wastes [J]. Hydrometallurgy, 2017, 167: 16−29.

[13] PATIÑO F, REYES I A, FLORES M U, PANDIYAN T, ROCA A, REYES M, HERNÁNDEZ J. Kinetic modeling and experimental design of the sodium arsenojarosite decomposition in alkaline media: Implications [J]. Hydrometallurgy, 2013, 137: 115−125.

[14] PAPPU A, THAKUR V K, PATIDAR R, ASOLEKAR S R, SAXENA M. Recycling marble wastes and jarosite wastes

into sustainable hybrid composite materials and validation through response surface methodology [J]. Journal of Cleaner Production, 2019, 240: 118249.

[15] MIRELES I, REYES I A, FLORES V H, PATIÑO F, FLORES M U, REYES M, ACOSTA M, CRUZ R, GUTIÉRREZ E J. Kinetic analysis of the decomposition of the $KFe_3(SO_4)_{2-x}(CrO_4)_x(OH)_6$ jarosite solid solution in Ca(OH)(2) medium[J]. Journal of the Brazilian Chemical Society, 2016, 27(6): 1014−1025.

[16] LIU C, JU S H, ZHANG L B, SRINIVASAKANNAN C, PENG J H, LE T Q X, GUO Z Y. Recovery of valuable metals from jarosite by sulphuric acid roasting using microwave and water leaching [J]. Canadian Metallurgical Quarterly, 2017, 56(1): 1−9.

[17] WU Jia-hui, CHAI Li-yuan, LIN Zhang, WEI Yang-jin, SHI Mei-qing, PENG Jun, PENG Ning, YAN Xu. Fe(II)-induced transformation of jarosite residues generated from zinc hydrometallurgy: Influence on metals behaviors during acid washing [J]. Hydrometallurgy, 2021, 200: 105523.

[18] MOMBELLI D, MAPELLI C, DI CECCA C, BARELLA S, GRUTTADAURIA A, RAGONA M, PISU M, VIOLA A. Characterization of cast iron and slag produced by jarosite sludges reduction via arc transferred plasma (ATP) reactor [J]. Journal of Environmental Chemical Engineering, 2018, 6(1): 773−783.

[19] STEINLECHNER S, ANTREKOWITSCH J. Thermodynamic considerations for a pyrometallurgical extraction of indium and silver from a jarosite residue [J]. Metals, 2018, 8(5): 335.

[20] WEGSCHEIDER S, STEINLECHNER S, LEUCHTENMÜLLER M. Innovative concept for the recovery of silver and indium by a combined treatment of jarosite and electric arc furnace dust [J]. JOM, 2017, 69(2): 388−394.

[21] RÄMÄ M, NURMI S, JOKILAAKSO A, KLEMETTINEN L, TASKINEN P, SALMINEN J. Thermal processing of jarosite leach residue for a safe disposable slag and valuable metals recovery [J], Metals, 2018, 8(10): 744.

[22] ZHU De-qing, YANG Cong-cong, PAN Jian, GUO Zheng-qi, LI Si-wei. New pyrometallurgical route for separation and recovery of Fe, Zn, In, Ga and S from jarosite residues [J]. Journal of Cleaner Production, 2018, 205: 781−788.

[23] XU Cui-min, XIE Qiao-qin, XU Fan, ZHOU Yue-fei, WANG Han-lin, CHEN Tian-hu, PENG Shu-chuan. Preparation of monoclinic pyrrhotite by thermal decomposition of jarosite residues and its heavy metal removal performance [J]. Minerals, 2021, 11(3): 267.

[24] GUO Zheng-qi, ZHAN Ruo-ning, SHI Yue, ZHU De-qing, PAN Jian, YANG Cong-cong, WANG Yi-ge, WANG Jin. Innovative and green utilization of zinc-bearing dust by hydrogen reduction: Recovery of zinc and lead, and synergetic preparation of Fe/C micro-electrolysis materials [J]. Chemical Engineering Journal, 2023, 456: 141157.

[25] JASZCZAK-FIGIEL B, GONTARZ Z. Stages of thermal decomposition of sodium oxo-salts of sulphur [J]. Journal of Thermal Analysis and Calorimetry, 2009, 96(1): 147−154.

[26] LEE S W, HONG K S, CONDRATE R A, HAPANOWICZ R P, SPEYER R F. Characterization of gas components and deposits in bubbles in silicate glasses prepared with sodium sulphate [J]. Journal of Materials Science, 1992, 27(18): 4961−4966.

[27] IKEDA O, KAINUMA R, OHNUMA I, FUKAMICHI K, ISHIDA K. Phase equilibria and stability of ordered b.c.c. phases in the Fe-rich portion of the Fe−Ga system [J]. Journal of Alloys and Compounds, 2002, 347(1/2): 198−205.

[28] LU Fang-hai, XIAO Tang-fu, LIN Jian, NING Zeng-ping, LONG Qiong, XIAO Li-hua, HUANG Fang, WANG Wan-kun, XIAO Qing-xiang, LAN Xiao-long, CHEN Hai-yan. Resources and extraction of gallium: A review [J]. Hydrometallurgy, 2017, 174: 105−115.

[29] FRENZEL M, KETRIS M P, SEIFERT T, GUTZMER J. On the current and future availability of gallium [J]. Resources Policy, 2016, 47: 38−50.

[30] JIN Bing-jie, DREISINGER D B. A green electrorefining process for production of pure lead from methanesulfonic acid medium [J]. Separation and Purification Technology, 2016, 170: 199−207.

[31] SHI Yuan, JIANG Kai-xi, ZHANG Ting-an, ZHU Xiao-feng. Simultaneous and clean separation of titanium, iron, and alumina from coal fly ash in one spot: Electrolysis-hydrolysis method [J]. Separation and Purification Technology, 2022, 294: 121247.

[32] SHI Yuan, JIANG Kai-xi, ZHANG Ting-an, ZHU Xiao-feng. Simultaneous separation of Fe & Al and extraction of Fe from waste coal fly ash: Altering the charge sequence of ions by electrolysis [J]. Waste Management, 2022, 137: 50−60.

基于氧化焙烧−直接还原−熔分−电解精炼工艺从铁矾渣中分步回收锌、铟、镓和铁

朱德庆[1]，董 韬[1]，潘 建[1]，郭正启[1]，杨聪聪[1]，薛钰霄[2]

1. 中南大学 资源加工与生物工程学院，长沙 410083；
2. 重庆大学 材料科学与工程学院，重庆 400045

摘 要：采用氧化焙烧−直接还原−熔炼−电解精炼工艺从典型有害铁矾渣中高效分离回收锌、铟、镓和铁。采用X 射线衍射(XRD)、热重−差热法(TG−DSC)和扫描电镜−能谱分析(SEM−EDS)对各分离过程中的相变及元素迁移进行表征。结果表明：铁矾渣在 1250 ℃氧化焙烧 20 min 后转变为赤铁矿和铁酸锌；将得到的氧化球团在 1200 ℃下还原 60 min，锌和铟挥发并富集于烟尘中；最后对还原球团进行熔炼及电解精炼分离铁和镓，得到铁含量为 99.5%的高纯铁粉和镓含量为 456 g/t 的富镓阳极泥。该工艺可实现锌、铟、铁和镓的总回收率分别为 97.42%、87.86%、90.70%和 84.78%。

关键词：铁矾渣; 镓；铟；回收；电解精炼

(Edited by Xiang-qun LI)